

Slow Hole Localization and Fast Electron Cooling in Cu-Doped InP/ZnSe Quantum Dots

P. Tim Prins, Dirk A. W. Spruijt, Mark J. J. Mangnus, Freddy T. Rabouw, Daniel Vanmaekelbergh, Celso de Mello Donega, and Pieter Geiregat*



Cite This: *J. Phys. Chem. Lett.* 2022, 13, 9950–9956



Read Online

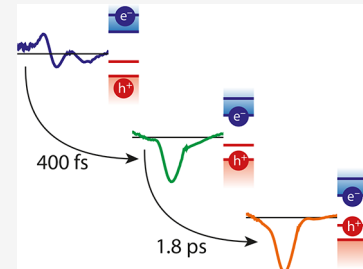
ACCESS |

Metrics & More

Article Recommendations

Supporting Information

ABSTRACT: Impurity doping of low-dimensional semiconductors is an interesting route towards achieving control over carrier dynamics and energetics, e.g., to improve hot carrier extraction, or to obtain strongly Stokes shifted luminescence. Such studies remain, however, underexplored for the emerging family of III–V colloidal quantum dots (QDs). Here, we show through a detailed global analysis of multiresonant pump–probe spectroscopy that electron cooling in copper-doped InP quantum dot (QDs) proceeds on subpicosecond time scales. Conversely, hole localization on Cu dopants is remarkably slow (1.8 ps), yet still leads to very efficient subgap emission. Due to this slow hole localization, common Auger assisted pathways in electron cooling cannot be blocked by Cu doping III–V systems, in contrast with the case of II–VI QDs. Finally, we argue that the structural relaxation around the Cu dopants, estimated to impart a reorganization energy of 220 meV, most likely proceeds simultaneously with the localization itself leading to efficient luminescence.



Owing to rapid developments in the last 30 years, colloidal semiconductor nanocrystals (quantum dots, QDs) are currently applied as luminophores in displays and lighting.¹ The promise of QDs extends beyond these applications; QDs may form the active building blocks for solution-processable lasers,² bioimagers, luminescent solar concentrators (LSC) and solar cells.³ QDs combine a certain ease of processing with size- and shape-dependent optoelectronic properties as observed in both the energetics and dynamics of charge carriers. A key process in carrier dynamics is carrier cooling after nonresonant photoexcitation. In applications that rely on the extraction of hot carriers, such as nonconventional photovoltaics and photocatalysis, this cooling is undesired.^{4,5} In many cases, however, fast cooling, i.e., on a femtosecond time scale, is observed,⁶ mostly facilitated by electron–hole coupled Auger mechanisms.^{7–10} In II–VI QDs, this dominant Auger cooling pathway can be blocked by fast trapping of valence band holes at doping-induced in-gap states leading to acclaimed multipicosecond hot electron lifetimes.^{11–13} Based on the above, the process of Cu-doping may also be a means to slow down hot-electron cooling in the more environmentally friendly family of III–V QDs, such as InP. Cu doping in InP QDs was shown to cause quenching of the band-edge emission and concomitant appearance of a broader, sub-bandgap emission.^{14–16} These changes in the steady state emission properties were ascribed to fast hole localization onto Cu⁺ dopants, followed by a structural lattice relaxation of the atoms around the Cu²⁺ site leading to strongly Stokes-shifted radiative recombination, similar to their II–VI counterparts.^{15,17,18} Even though hole localization most likely occurs in III–V systems, for this to lead to a blocking of the Auger

process critically depends on the time scale of electron–hole Auger coupling compared to the extraction of holes from the valence band by trapping. To date, the time scales of the assumed hole localization with respect to electron cooling remain unknown. It is therefore unclear whether the concept of slowing down electron cooling via doping also applies to the emerging family of III–V QDs with restricted toxicity.

Besides its effect on Auger electron–hole coupling, impurity doping enables sub-band gap luminescence.¹⁹ The Stokes shift can be considerable and depends on the energetics and dynamics of the structural reorganization around the trapped carrier. Impurity-induced emission with a high quantum yield is much desired in LSCs in order to avoid photon losses by reabsorption in the QD luminophores.^{20,21} In laser materials, the impurity level can result in population inversion and gain due to the large Stokes shift, similar to what is found in organic dyes.²² So far, the understanding of charge-induced structural reorganization remains limited, in particular for III–V QDs.

In this work, we study the effect of Cu doping on the charge-carrier cooling dynamics in InP QDs. We use broadband and ultrafast pump–probe transient absorption (TA) spectroscopy with a range of different excitation wavelengths, chosen to be resonant with the relevant optical transitions. This method is

Received: September 7, 2022

Accepted: October 14, 2022

Published: October 19, 2022



ideally suited to investigate hot-carrier dynamics on the relevant time and energy scales.²³ However, as the simultaneous occurrence of transient bleaches, spectral shifts and induced absorptions observed in such experiments make data interpretation very difficult, we proceeded to employ an unbiased global-fit analysis method to identify excited states and quantify their dynamics in the context of cooling and structural reorganization.^{24–29} As opposed to Cu-doped II–VI systems, we find that electron cooling in Cu:InP proceeds on ultrafast subpicosecond time scales whereas hole localization on Cu⁺ in InP QDs occurs on a much slower, multipicosecond, time scale. Hence, Cu dopants in InP quantum dots are most likely not able to prevent commonly observed Auger-assisted carrier cooling and are surprisingly ineffective as a strategy to slow down hot carriers. Hole localization onto Cu⁺ leads to Cu²⁺, which shows a strong reorganization energy. We do not observe this effect separately from the relaxation within our time resolution (ca. 150 fs), which suggests the process is extremely fast and most likely overlaps temporally with the hole localization itself, thereby finally leading to the observed efficient Stokes shifted emission.

Cu-doped and undoped InP/ZnSe/ZnSe_{0.5}S_{0.5}/ZnS core-shell QDs, consisting of a ~3 nm InP core and a 3 monolayer shell, were prepared following a synthesis procedure adapted from literature,¹⁴ see Methods in the Supporting Information (SI) and optical characterization of the InP cores in Figure S1. For simplicity, the explicit specification of the QD shells will be omitted hereafter. Inductively coupled plasma optical emission spectrometry (ICP-OES) on thoroughly washed core/shell samples shows that the Cu-doped InP QDs contain on average 30 Cu atoms per QD (SI S1). Both higher and lower doping levels were checked but results are always in line with what follows.

The absorption spectrum of the undoped InP QDs shows features at 2.2 and 2.7 eV (Figure 1a), which are assigned to transitions from the 1S_h and 1P_h level in the valence band (VB) to the 1S_e and 1P_e level in the conduction band (CB), respectively.³² The emission spectrum shows band-edge emission at 2.1 eV with a broad tail to lower energies related to trap states^{33,34} (Figure 1a). Upon Cu doping, the absorption peaks broaden and an absorption shoulder appears at lower

energy, which is assigned to the excitation of Cu⁺ d-electrons to the CB.^{15,35,36} Such impurity-related absorption is often very low in oscillator strength, but can be clearly resolved here with an oscillator strength about 1 order of magnitude below the band edge absorption. Moreover, the band-edge emission is quenched, while a broad emission peak appears at 1.47 eV (Figure 1a). The resulting shift between the absorption peak at 2.2 eV and the emission is usually referred to as the apparent or global Stokes shift,^{37,38} here 0.74 eV. The emission observed in Cu-doped InP QDs has a photoluminescence (PL) lifetime of 480 ns (Figure 1b and Figure S3a) with a quantum yield of 40%, which is much longer than that of the band-edge emission in undoped InP QDs (viz., 40 ns, Figure 1b and Figure S3b). The ratio of the two lifetimes (480/40) matches the expected ratio of oscillator strengths obtained from absorption, being 1 order of magnitude, indicating little competition with nonradiative channels for the Cu-localized exciton. These observations are consistent with previous results on Cu-doped QDs¹⁷ and allow us to assign the emission observed in Cu:InP QDs to the radiative recombination of a Cu-localized hole with a delocalized CB electron.

Figure 2a shows the normalized transient absorption (ΔA) spectra for Cu-doped and undoped InP QDs at 1 ns after excitation at 3.1 eV. At this delay time, all carriers have relaxed to their lowest excited state but have not yet recombined radiatively, as the PL decay time is much longer at 40 ns for undoped or 480 ns for doped QDs (Figure 1b). Both spectra show a negative signal (bleach) at 2.2 eV, matching the 1S_h–1S_e transition observed in the steady-state absorption spectra (Figure 1a). This transition is bleached in both the Cu-doped and undoped InP QDs; this can be understood by seeing that, in both cases, the lowest excited state has an electron-occupied 1S_e level. The TA spectrum of the Cu-doped InP QDs shows an additional bleach around 1.9 eV, which is absent in the TA spectrum of undoped QDs. This transition is also observed in the steady-state absorption spectrum of Cu-doped InP QDs, where it is assigned to the excitation of a Cu⁺ d-electron to the 1S_e CB level, creating a Cu²⁺–1S_e excited state. Consequently, occupation of the 1S_e level bleaches this transition (Figure 2b). Besides negative signatures, both spectra also show a positive signal (photoinduced absorption) in the near-infrared region with a similar amplitude, from 1.0 to 1.7 eV (Figure 2a). This induced absorption is assigned to intraband transitions involving the excitation of the photogenerated electron and hole to higher CB and VB states, respectively.³⁹ The induced absorption does not show any significant kinetics on the time scale of the experiment (up to 3 ns) and appears instantly after excitation.

To determine the energies of the 1S_h–1S_e and the Cu²⁺–1S_e excited states, we fitted the bleach spectrum of the Cu-doped InP QDs to two Gaussians (Figure 2d). The transitions are broadened due to variations in size, shape, and composition of the QDs, surface imperfections that affect excited-state energies,³⁰ possible fine-structure splitting, and finally electron–phonon coupling.⁴⁰ The absorbing and emitting transitions between the ground state and the Cu²⁺–1S_e excited state are particularly broad (Figure 2d), mainly because the localized nature of the hole increases phonon coupling.¹⁵ The shift between the maxima of the Cu⁺ to 1S_e bleach (Figure 2d, orange dashed line) and the emission, i.e., the Stokes shift, is 440 meV (Figure 2d, red line). Within the framework of a generalized Marcus model, this energy shift is twice the reorganization energy of the lattice for accommodating the

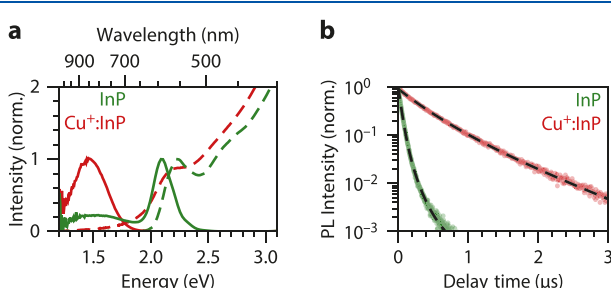


Figure 1. Linear Optical Properties. (a) Absorption (dashed) and emission (solid) spectra of Cu-doped (red) and undoped InP (green) QDs. Both QDs have a ZnSe/ZnSe_{0.5}S_{0.5}/ZnS shell. The absorption spectra are normalized at 4.1 eV (Figure S2). The fwhm of the emission from the Cu-doped and undoped QDs is 350 and 200 meV, respectively. (b) Photoluminescence decay curves of Cu-doped (red) and undoped InP (green) QDs under 515 nm excitation, taken at their respective emission maxima. The dashed lines show fits to a model for recombination between a delocalized electron and a localized hole³⁰ and a model of single exponential decay and delayed emission,³¹ respectively (Figure S3).

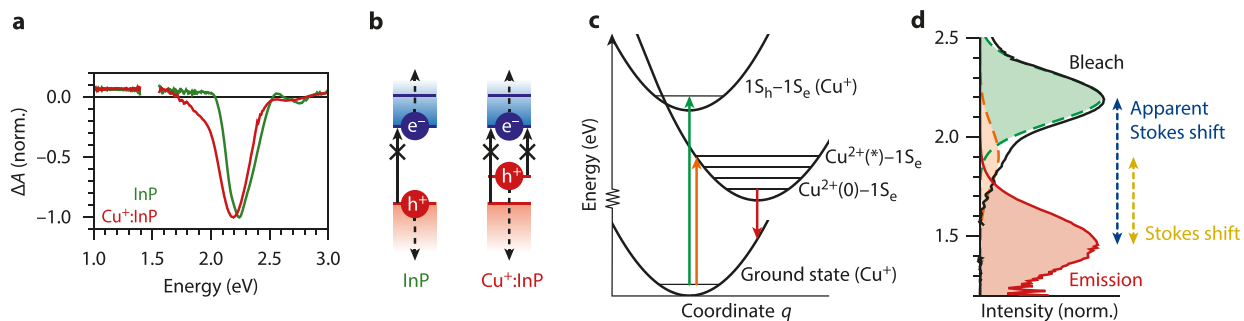


Figure 2. Energetics of absorption and emission. (a) Normalized TA spectra of Cu-doped (red) and undoped InP QDs (green) after carrier cooling (1 ns delay time). (b) Schematic representation of the transitions that are blocked (solid arrows with cross) and new excited-state absorption transitions (dashed arrows). (c) Configurational diagrams of the ground and excited many-body states involved in excitation, cooling, trapping, and emission (not to scale and only some vibrational levels are shown). The coordinate q represents the environment around the Cu site. (d) The TA spectrum of the Cu-doped InP QDs decomposed into contributions of a VB to CB bleach (green) and a Cu^+ to CB bleach (orange). The emission spectrum is shown in red. The apparent and real Stokes shift are indicated with the blue and yellow arrows, they are 0.74 and 0.44 eV, respectively.

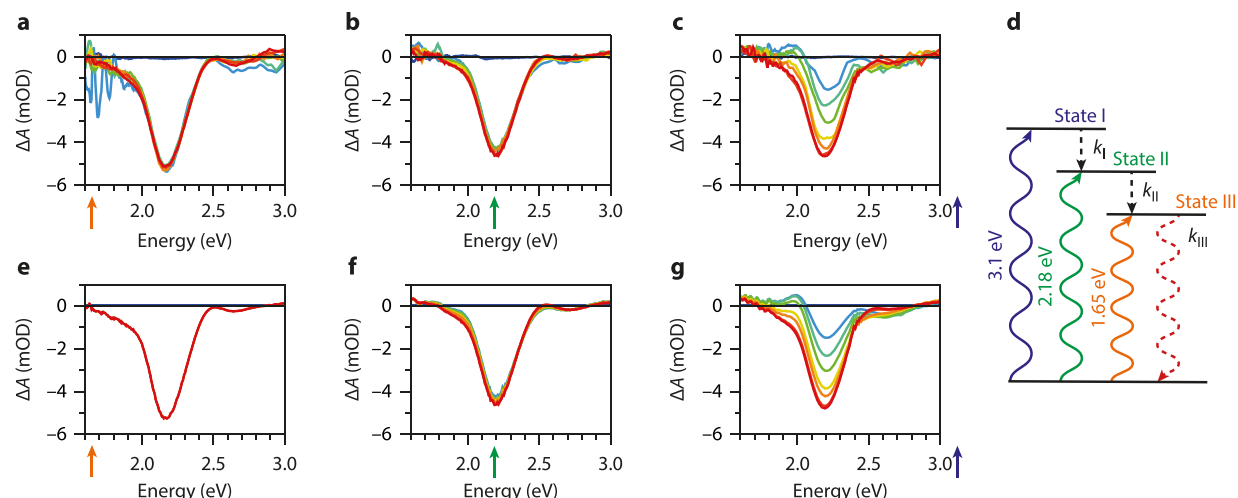


Figure 3. Multiresonant TA spectroscopy. (a–c) Experimental transient absorption spectra of Cu-doped InP QDs at different delay times (−1, 0.1, 0.3, 0.5, 1, 1.5, 7 ps from blue to red) normalized for the absorbed fluence (SI S2). The QDs are excited at (a) 1.65 eV, (b) 2.18 eV, and (c) 3.1 eV. (d) An overview of the excited states created with the three different excitation energies, respectively blue, green, and orange. k_I and k_{II} are cooling processes and k_{III} is the final radiative recombination (dashed red arrow). (e–g) Global fit results from the data shown in panels a–c, using the model depicted in panel d. The arrows in panels (a–c, e–g) indicate the excitation energy with the same color coding as in panel d.

change in the effective Cu oxidation state upon localization of the photogenerated hole. This reorganization energy of 220 meV is in line with reports on other Cu-containing QDs and DFT predictions on II–VI clusters.^{15,35} The vibrational-zero level of the $\text{Cu}^{2+}(0)-1S_e$ excited state is in the middle between the maxima of absorption and emission, which is at 1.7 eV, see Figure 2d. We estimate the energy of the $1S_h-1S_e$ excited state from the energy of the maximum of the corresponding bleach feature (Figure 2d, green dashed line) at 2.2 eV.

By exciting the InP QDs with different pump wavelengths, we can create various excited-state configurations and follow their decay pathways. A pump pulse with an energy of 1.65 eV excites Cu-doped InP QDs selectively (resonantly) in the Cu^+ -to- $1S_e$ transition (Figure 2c, orange arrow). Figure 3a shows the resulting TA spectra, measured at different delay times, −1 ps and between 0.1 and 7 ps (Figure S4a for 2D heatmap). The shape of the spectrum is independent of delay time and shows the absorption bleach of the $\text{Cu}^+ \rightarrow 1S_e$ and the $1S_h \rightarrow 1S_e$ transitions that we identified before (Figure 2c,d). This is consistent with instantaneous, i.e., within our time resolution, formation of the $\text{Cu}^{2+}-1S_e$ excited state, from which radiative

decay is slower than the time range of 3 ns available with our TA Instrument (Figure 1b).

Shorter pump wavelengths produce TA spectra that change over the first few ps after excitation (Figure 3b,c). Excitation with 2.18 eV, which matches the $1S_h$ -to- $1S_e$ transition (Figure 2c, green arrow), results in minor spectral changes over the first few picoseconds most notably in the tail of the absorption bleach at 1.9 eV (Figure 3b, Figure S4b for 2D heatmap). After a few picoseconds, the TA spectrum excited with 2.18 eV is the same as that excited with 1.65 eV (Figure 3a). We conclude that the dynamics in the first few picoseconds are most likely due to relaxation from the $1S_h-1S_e$ excited state to the $\text{Cu}^{2+}-1S_e$ excited state that we pumped in Figure 3a.

Continuing our systematic variation of pump wavelength, we excite nonresonantly at 3.1 eV. This results in an early time TA spectrum with multiple positive and negative signals (Figure 3c, Figure S4c for 2D heatmap). Within <1 ps, the spectrum converges to the early time spectrum that we saw before in Figure 3b, after which it changes further to resemble the spectra seen in Figure 3a. This is consistent with initial creation of an excited state with excess charge-carrier energy, which first

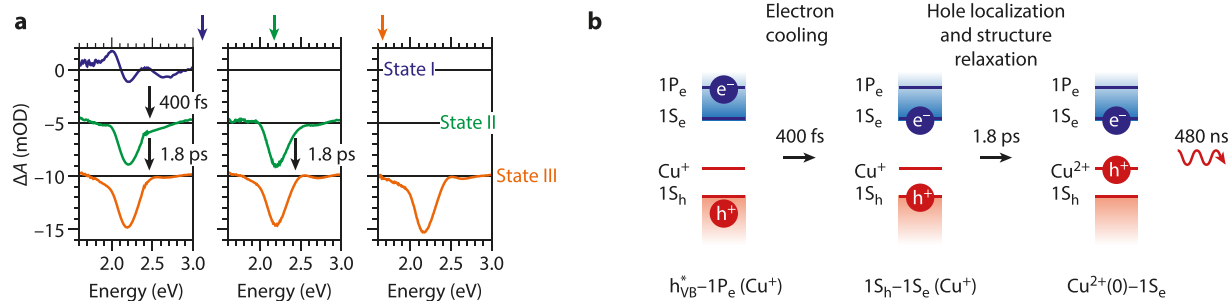


Figure 4. Global Fit Analysis. (a) The transient absorption spectra of excited states I (blue), II (green), and III (orange) in Cu-doped InP QDs obtained from the global-fit analysis method for the three different excitation energies: blue arrow for 3.1 eV, green arrow for 2.18 eV, and orange arrow for 1.65 eV excitation. The spectra are shifted with -5 mOD for clarity. The black arrows show the fitted time constants for the transitions between the excited states. (b) Schematic representation of how we interpret the three excited states, $h_{VB}^*-1P_e(\text{Cu}^+)$, $1S_h-1S_e(\text{Cu}^+)$, and $\text{Cu}^{2+}(0)-1S_e$ respectively, and their lifetimes.

relaxes to the $1S_h-1S_e$ excited state that we pumped in Figure 3b, and then further to the $\text{Cu}^{2+}-1S_e$ excited state that we created in Figure 3a.

When the spectral changes are as intricate as in Figure 3c, it is challenging to quantitatively understand the cooling dynamics from single-wavelength kinetic analysis. To retrieve the spectral signatures of the different excited states and quantify their lifetimes, we used an unbiased global fit analysis method with the kinetic model depicted in Figure 3d (see SI S4 for rate equations and fitting procedure). The spectra from the global fit are given in Figures 3e–g for the Cu-doped and undoped InP QDs, respectively. Comparing the experimental TA spectra (Figures 3a–c) to the fitted spectra (Figure 3e–g), we see that the agreement is excellent. Same, when we plot the data and global fit results as a function of time for specific energies, which can be found in Figure S5.

From our global-fit procedure, we can reconstruct the pure transient absorption spectra of the excited states involved. Important to note is that we do not input these spectra into the global fit but instead, they are an unbiased outcome of the fitting procedure. The spectra of the excited states of Cu-doped InP QDs for the three different excitation energies are shown in Figure 4a. The spectra of the excited state III are very comparable for the three different excitation energies (Figure 4a (lowest row), see also Figure S6). As discussed above, excited state III must be the $\text{Cu}^{2+}-1S_e$ state, which we create instantaneously when pumping at 1.65 eV (Figure 2c, orange arrow). This state could in principle be a vibrationally excited state of the Cu^{2+} , say $\text{Cu}^{2+}(*)$ in Figure 2c, or directly the vibrational ground state $\text{Cu}^{2+}(0)$. Both should be separated by the reorganization energy, but no such distinct set of spectra is obtained from the global fit. This indicates that the process of reorganization is faster than our time resolution, happening hence in concert with the hole localization itself. Arguing this reorganization is slower than our 3 ns time window is countered by the observation that the transient Stokes shifted PL grows in instantly, apart from the 150 ps time resolution, as is shown in Figure S3b.

The spectra of excited state II, which is the intermediate state under 3.1 eV excitation and the initial state under 2.18 eV excitation, are also remarkably similar for the two excitation wavelengths (Figure 4a (middle row), see also Figure S7). Note: in the 2.18 eV experiment we created 55% of excited state II and 45% of excited state III at $t = 0$, due to overlap of the absorbing transitions (Figure 2d, green and orange dashed lines). The striking similarity between the spectra confirms that

after nonresonant excitation (3.1 eV excitation), the system initially relaxes to the same excited state that we create by excitation at 2.18 eV. We therefore interpret excited state II as the $1S_h-1S_e$ state, which we excite resonantly at 2.18 eV (Figure 2c, green arrow) and in which both the hole and electron occupy a delocalized band-edge level. We emphasize again that our global-fit procedure does not impose these similarities of the spectra a priori. The changes in the TA spectra between excited states II and III are induced by the hole localization on Cu which shows up as an extra bleach at 2.1 eV. Previous work on CdSe-based QDs has shown that a hole with excess energy can induce a photoinduced absorption on the lower energy side of the $1S_h-1S_e$ bleach (Figure S8).^{41,42} Such a positive signal can partially cancel the bleach of the Cu^+ to $1S_e$ transition. The difference between the TA spectra of excited states II and III is likely due to the disappearance of such a type of additional induced absorption feature at 1.9 eV, because the hole cools, i.e., loses its excess energy, when localizing on Cu. As argued above, we only observe one final state for the localized hole, indicating that any structural relaxation occurs either in concert with or faster than our time resolution.

The highest excited state I of Cu-doped InP QDs (Figure 4a (top row)) produces a derivative-like feature around the band gap energy at 2.1 eV and a bleach around 2.7 eV. This looks similar to the initial excited state we observe when performing the same measurement on the equally sized but undoped InP-based core/shell QDs (steady-state measurements in Figure 1a, TA measurements in Figure S9). The bleach at 2.7 eV matches well with the higher energy feature observed in the steady-state absorption spectrum (Figure 1a), which is assigned to a transition from the $1P_h$ -level in the VB to the $1P_e$ -level in the CB.³² For this reason, we assign the highest excited state I populated under 3.1 eV to a situation where the electron occupies the $1P_e$ level. The electron occupation of the $1P_e$ level typically results in a red-shifted $1S_h \rightarrow 1S_e$ transition, resulting in the derivative-like feature in the differential absorption spectrum at 2.1 eV, as observed very clearly here.^{23,41} Even though it is difficult to label exactly the hole level in the excited state, we can assume that the hole is delocalized over the dense hole manifold. For these reasons, we choose the label $h_{VB}^*-1P_e$ in Figure 4b, to indicate that the carriers are in the bands with excess energy compared to the band edge.

Our global-fit analysis for different excitation wavelengths unambiguously shows that hole localization from the VB edge ($1S_h$ state) to a Cu^+ dopant is remarkably slow (1.8 ps), in

particular compared to typical time scales for hot-electron cooling from the 1P level (<500 fs).^{43–47} Indeed, the time constant for hot-carrier cooling for our undoped InP-based core/shell QDs is 250 fs (see SI Figure S9). The photo-generated hole in both undoped and Cu-doped InP-based core/shell QDs therefore remains delocalized during the cooling process (Figure 4b). Hence, Cu doping cannot prevent any potential involvement of electron–hole Auger coupling in the cooling process. This explains why hot electrons created under 3.1 eV excitation relax in only 400 fs, comparable to the lifetime in the undoped InP QDs. This conclusion is in stark contrast with the earlier interpretation of TA data on Cu-doped CdSe QDs.¹³ The authors of ref 13 attributed a slower component in the kinetics to slow electron cooling following ultrafast hole localization onto Cu. Our results based on a detailed global analysis, however, show that this strategy does not work for InP QDs. As to the microscopic nature of the very different coupling between the delocalized hole wave function and the Cu-sites in II–VI vs. III–V systems, we can only hypothesize at this point. A luminescence lifetime-fitting model, shown in Figure S3(c), indicates that Cu-atoms are most likely very uniformly distributed in large amounts throughout the InP core. Together with the dominantly type I band alignment in InP/ZnSe, this suggests that strong spatial overlap exists between Cu-sites and the initial band-edge hole wave function. If Cu dopants spread differently in the CdSe-based systems, one could expect a different degree of coupling leading to the observed fast hole localization. This thereby raises the question how electron cooling in the technologically relevant and environmentally friendly family of III–V materials can be slowed down. Combining Cu-doping with other ways of reducing the Auger cooling rate, e.g., thick and/or type-II core–shell architectures,^{48–51} might be key to significantly increase the lifetime of the hot electron.

To conclude, a rigorous analysis of multiresonant TA spectroscopic studies on Cu-doped and undoped InP-based core/shell QDs demonstrates that localization of the photo-generated hole in Cu-doped InP QDs is slow, with a time constant of 1.8 ps, thereby preventing any slowdown of carrier relaxation of hot electrons. Our results further identify that structural relaxation of the Cu site is most likely ultrafast with a reorganization energy of 220 meV.

ASSOCIATED CONTENT

Supporting Information

The Supporting Information is available free of charge at <https://pubs.acs.org/doi/10.1021/acs.jpcllett.2c02764>.

Additional data, methods for the normalization procedure and global fit analysis, and transient absorption spectroscopy data on undoped InP-based core/shell QDs ([PDF](#))

AUTHOR INFORMATION

Corresponding Author

Pieter Geiregat – Department of Chemistry, Ghent University, 9000 Gent, Belgium; orcid.org/0000-0001-7217-8738; Email: pieter.geiregat@ugent.be

Authors

P. Tim Prins – Debye Institute for Nanomaterials Science, Utrecht University, 3584CC Utrecht, The Netherlands; orcid.org/0000-0002-8258-0074

Dirk A. W. Spruijt – Debye Institute for Nanomaterials Science, Utrecht University, 3584CC Utrecht, The Netherlands

Mark J. J. Mangnus – Debye Institute for Nanomaterials Science, Utrecht University, 3584CC Utrecht, The Netherlands; orcid.org/0000-0002-3595-8097

Freddy T. Rabouw – Debye Institute for Nanomaterials Science, Utrecht University, 3584CC Utrecht, The Netherlands; orcid.org/0000-0002-4775-0859

Daniel Vanmaekelbergh – Debye Institute for Nanomaterials Science, Utrecht University, 3584CC Utrecht, The Netherlands; orcid.org/0000-0002-3535-8366

Celso de Mello Donega – Debye Institute for Nanomaterials Science, Utrecht University, 3584CC Utrecht, The Netherlands; orcid.org/0000-0002-4403-3627

Complete contact information is available at:
<https://pubs.acs.org/10.1021/acs.jpcllett.2c02764>

Notes

The authors declare no competing financial interest.

ACKNOWLEDGMENTS

P.T.P., D.V., and C.D.M.D. acknowledge support by The Netherlands Organization for Scientific Research (NWO; grant 14614 “Q-Lumicon”).

REFERENCES

- (1) Won, Y.-H.; Cho, O.; Kim, T.; Chung, D.-Y.; Kim, T.; Chung, H.; Jang, H.; Lee, J.; Kim, D.; Jang, E. Highly Efficient and Stable InP/ZnSe/ZnS Quantum Dot Light-Emitting Diodes. *Nature* **2019**, *575*, 634–638.
- (2) Geiregat, P.; Van Thourhout, D.; Hens, Z. A Bright Future for Colloidal Quantum Dot Lasers. *NPG Asia Mater.* **2019**, *11*, 41.
- (3) Kovalenko, M. V.; Manna, L.; Cabot, A.; Hens, Z.; Talapin, D. V.; Kagan, C. R.; Klimov, V. I.; Rogach, A. L.; Reiss, P.; Milliron, D. J.; Guyot-Sionnest, P.; Konstantatos, G.; Parak, W. J.; Hyeon, T.; Korgel, B. A.; Murray, C. B.; Heiss, W. Prospects of Nanoscience with Nanocrystals. *ACS Nano* **2015**, *9*, 1012–1057.
- (4) Clavero, C. Plasmon-Induced Hot-Electron Generation at Nanoparticle/Metal-Oxide Interfaces for Photovoltaic and Photocatalytic Devices. *Nat. Photonics* **2014**, *8*, 95–103.
- (5) Grimaldi, G.; Crisp, R. W.; ten Brinck, S.; Zapata, F.; van Ouwendorp, M.; Renaud, N.; Kirkwood, N.; Evers, W. H.; Kinge, S.; Infante, I.; Siebbeles, L. D. A.; Houtepen, A. J. Hot-Electron Transfer in Quantum-Dot Heterojunction Films. *Nat. Commun.* **2018**, *9*, 2310.
- (6) Rabouw, F. T.; de Mello Donega, C. Excited-State Dynamics in Colloidal Semiconductor Nanocrystals. *Top. Curr. Chem.* **2016**, *374*, 58.
- (7) Efros, A. L.; Kharchenko, V. A.; Rosen, M. Breaking the Phonon Bottleneck in Nanometer Quantum Dots: Role of Auger-like Processes. *Solid State Commun.* **1995**, *93*, 281–284.
- (8) Klimov, V. I.; McBranch, D. W. Femtosecond 1P-to-1S Electron Relaxation in Strongly Confined Semiconductor Nanocrystals. *Phys. Rev. Lett.* **1998**, *80*, 4028–4031.
- (9) Guyot-Sionnest, P.; Shim, M.; Matranga, C.; Hines, M. Intraband Relaxation in CdSe Quantum Dots. *Phys. Rev. B* **1999**, *60*, R2181–R2184.
- (10) Klimov, V. I.; Mikhailovsky, A. A.; McBranch, D. W.; Leatherdale, C. A.; Bawendi, M. G. Mechanisms for Intraband Energy Relaxation in Semiconductor Quantum Dots: The Role of Electron-Hole Interactions. *Phys. Rev. B* **2000**, *61*, R13349–R13352.
- (11) Maiti, S.; Dana, J.; Jadhav, Y.; Debnath, T.; Haram, S. K.; Ghosh, H. N. Electrochemical Evaluation of Dopant Energetics and the Modulation of Ultrafast Carrier Dynamics in Cu-Doped CdSe Nanocrystals. *J. Phys. Chem. C* **2017**, *121*, 27233–27240.

- (12) Dutta, A.; Bera, R.; Ghosh, A.; Patra, A. Ultrafast Carrier Dynamics of Photo-Induced Cu-Doped CdSe Nanocrystals. *J. Phys. Chem. C* **2018**, *122*, 16992–17000.
- (13) Wang, L.; Chen, Z.; Liang, G.; Li, Y.; Lai, R.; Ding, T.; Wu, K. Observation of a Phonon Bottleneck in Copper-Doped Colloidal Quantum Dots. *Nat. Commun.* **2019**, *10*, 4532.
- (14) Xie, R.; Peng, X. Synthesis of Cu-Doped InP Nanocrystals (d-Dots) with ZnSe Diffusion Barrier as Efficient and Color-Tunable NIR Emitters. *J. Am. Chem. Soc.* **2009**, *131*, 10645–10651.
- (15) Knowles, K. E.; Nelson, H. D.; Kilburn, T. B.; Gamelin, D. R. Singlet–Triplet Splittings in the Luminescent Excited States of Colloidal Cu⁺:CdSe, Cu⁺:InP, and CuInS₂ Nanocrystals: Charge-Transfer Configurations and Self-Trapped Excitons. *J. Am. Chem. Soc.* **2015**, *137*, 13138–13147.
- (16) Mundy, M. E.; Eagle, F. W.; Hughes, K. E.; Gamelin, D. R.; Cossairt, B. M. Synthesis and Spectroscopy of Emissive, Surface-Modified, Copper-Doped Indium Phosphide Nanocrystals. *ACS Mater. Lett.* **2020**, *2*, 576–581.
- (17) Knowles, K. E.; Hartstein, K. H.; Kilburn, T. B.; Marchioro, A.; Nelson, H. D.; Whitham, P. J.; Gamelin, D. R. Luminescent Colloidal Semiconductor Nanocrystals Containing Copper: Synthesis, Photophysics, and Applications. *Chem. Rev.* **2016**, *116*, 10820–10851.
- (18) Hassan, A.; Zhang, X.; Liu, C.; Snee, P. T. Electronic Structure and Dynamics of Copper-Doped Indium Phosphide Nanocrystals Studied with Time-Resolved X-Ray Absorption and Large-Scale DFT Calculations. *J. Phys. Chem. C* **2018**, *122*, 11145–11151.
- (19) Norris, D. J.; Efros, A. L.; Erwin, S. C. Doped Nanocrystals. *Science* **2008**, *319*, 1776–1779.
- (20) Bradshaw, L. R.; Knowles, K. E.; McDowall, S.; Gamelin, D. R. Nanocrystals for Luminescent Solar Concentrators. *Nano Lett.* **2015**, *15*, 1315–1323.
- (21) Sadeghi, S.; Bahmani Jalali, H.; Srivastava, S. B.; Melikov, R.; Baylam, I.; Sennaroglu, A.; Nizamoglu, S. High-Performance, Large-Area, and Ecofriendly Luminescent Solar Concentrators Using Copper-Doped InP Quantum Dots. *iScience* **2020**, *23*, 101272.
- (22) Geiregat, P.; Houtepen, A. J.; Sagar, L. K.; Infante, I.; Zapata, F.; Grigel, V.; Allan, G.; Delerue, C.; Van Thourhout, D.; Hens, Z. Continuous-Wave Infrared Optical Gain and Amplified Spontaneous Emission at Ultralow Threshold by Colloidal HgTe Quantum Dots. *Nat. Mater.* **2018**, *17*, 35–42.
- (23) Klimov, V. I.; McBranch, D. W. Femtosecond High-Sensitivity, Chirp-Free Transient Absorption Spectroscopy Using Kilohertz Lasers. *Opt. Lett.* **1998**, *23*, 277–279.
- (24) McArthur, E. A.; Morris-Cohen, A. J.; Knowles, K. E.; Weiss, E. A. Charge Carrier Resolved Relaxation of the First Excitonic State in CdSe Quantum Dots Probed with Near-Infrared Transient Absorption Spectroscopy. *J. Phys. Chem. B* **2010**, *114*, 14514–14520.
- (25) Knowles, K. E.; McArthur, E. A.; Weiss, E. A. A Multi-Timescale Map of Radiative and Nonradiative Decay Pathways for Excitons in CdSe Quantum Dots. *ACS Nano* **2011**, *5*, 2026–2035.
- (26) Ashner, M. N.; Winslow, S. W.; Swan, J. W.; Tisdale, W. A. Markov Chain Monte Carlo Sampling for Target Analysis of Transient Absorption Spectra. *J. Phys. Chem. A* **2019**, *123*, 3893–3902.
- (27) Labrador, T.; Dukovic, G. Simultaneous Determination of Spectral Signatures and Decay Kinetics of Excited State Species in Semiconductor Nanocrystals Probed by Transient Absorption Spectroscopy. *J. Phys. Chem. C* **2020**, *124*, 8439–8447.
- (28) van Stokkum, I. H. M.; Larsen, D. S.; van Grondelle, R. Global and Target Analysis of Time-Resolved Spectra. *Biochim. Biophys. Acta - Bioenerg.* **2004**, *1657*, 82–104.
- (29) Ruckebusch, C.; Sliwa, M.; Pernot, P.; de Juan, A.; Tauler, R. Comprehensive Data Analysis of Femtosecond Transient Absorption Spectra: A Review. *J. Photochem. Photobiol. C Photochem. Rev.* **2012**, *13*, 1–27.
- (30) Hinterding, S. O. M.; Mangnus, M. J. J.; Prins, P. T.; Jöbsis, H. J.; Busatto, S.; Vanmaekelbergh, D.; de Mello Donega, C.; Rabouw, F. T. Unusual Spectral Diffusion of Single CuInS₂ Quantum Dots Sheds Light on the Mechanism of Radiative Decay. *Nano Lett.* **2021**, *21*, 658–665.
- (31) Rabouw, F. T.; Kamp, M.; van Dijk-Moes, R. J. A.; Gamelin, D. R.; Koenderink, A. F.; Meijerink, A.; Vanmaekelbergh, D. Delayed Exciton Emission and Its Relation to Blinking in CdSe Quantum Dots. *Nano Lett.* **2015**, *15*, 7718–7725.
- (32) Fu, H.; Zunger, A. Excitons in InP Quantum Dots. *Phys. Rev. B* **1998**, *57*, R15064–R15067.
- (33) Guzelian, A. A.; Katari, J. E. B.; Kadavanich, A. V.; Banin, U.; Hamad, K.; Juban, E.; Alivisatos, A. P.; Wolters, R. H.; Arnold, C. C.; Heath, J. R. Synthesis of Size-Selected, Surface-Passivated InP Nanocrystals. *J. Phys. Chem.* **1996**, *100*, 7212–7219.
- (34) Mićić, O. I.; Sprague, J.; Lu, Z.; Nozik, A. J. Highly Efficient Band-edge Emission from InP Quantum Dots. *Appl. Phys. Lett.* **1996**, *68*, 3150–3152.
- (35) Nelson, H. D.; Li, X.; Gamelin, D. R. Computational Studies of the Electronic Structures of Copper-Doped CdSe Nanocrystals: Oxidation States, Jahn–Teller Distortions, Vibronic Bandshapes, and Singlet–Triplet Splittings. *J. Phys. Chem. C* **2016**, *120*, 5714–5723.
- (36) Nelson, H. D.; Hinterding, S. O. M.; Fainblat, R.; Creutz, S. E.; Li, X.; Gamelin, D. R. Mid-Gap States and Normal vs Inverted Bonding in Luminescent Cu⁺- and Ag⁺-Doped CdSe Nanocrystals. *J. Am. Chem. Soc.* **2017**, *139*, 6411–6421.
- (37) Fuhr, A.; Yun, H. J.; Crooker, S. A.; Klimov, V. I. Spectroscopic and Magneto-Optical Signatures of Cu¹⁺ and Cu²⁺ Defects in Copper Indium Sulfide Quantum Dots. *ACS Nano* **2020**, *14*, 2212–2223.
- (38) Berends, A. C.; Mangnus, M. J. J.; Xia, C.; Rabouw, F. T.; de Mello Donega, C. Optoelectronic Properties of Ternary I–III–VI 2 Semiconductor Nanocrystals: Bright Prospects with Elusive Origins. *J. Phys. Chem. Lett.* **2019**, *10*, 1600–1616.
- (39) Guyot-Sionnest, P.; Hines, M. A. Intraband Transitions in Semiconductor Nanocrystals. *Appl. Phys. Lett.* **1998**, *72*, 686–688.
- (40) Cui, J.; Beyler, A. P.; Coropceanu, I.; Cleary, L.; Avila, T. R.; Chen, Y.; Cordero, J. M.; Heathcote, S. L.; Harris, D. K.; Chen, O.; Cao, J.; Bawendi, M. G. Evolution of the Single-Nanocrystal Photoluminescence Linewidth with Size and Shell: Implications for Exciton–Phonon Coupling and the Optimization of Spectral Linewidths. *Nano Lett.* **2016**, *16*, 289–296.
- (41) Hwang, Y.-N.; Je, K.-C.; Kim, D.; Park, S.-H. Observation of Enhanced Biexciton Effect in Semiconductor Nanocrystals. *Phys. Rev. B* **2001**, *64*, 041305.
- (42) Grimaldi, G.; Geuchies, J. J.; van der Stam, W.; du Fossé, I.; Brynjarsdóttir, B.; Kirkwood, N.; Kinge, S.; Siebbeles, L. D. A.; Houtepen, A. J. Spectroscopic Evidence for the Contribution of Holes to the Bleach of Cd-Chalcogenide Quantum Dots. *Nano Lett.* **2019**, *19*, 3002–3010.
- (43) Ellingson, R. J.; Blackburn, J. L.; Yu, P.; Rumbles, G.; Mićić, O. I.; Nozik, A. J. Excitation Energy Dependent Efficiency of Charge Carrier Relaxation and Photoluminescence in Colloidal InP Quantum Dots. *J. Phys. Chem. B* **2002**, *106*, 7758–7765.
- (44) Blackburn, J. L.; Ellingson, R. J.; Mićić, O. I.; Nozik, A. J. Electron Relaxation in Colloidal InP Quantum Dots with Photo-generated Excitons or Chemically Injected Electrons. *J. Phys. Chem. B* **2003**, *107*, 102–109.
- (45) Richter, A. F.; Binder, M.; Bohn, B. J.; Grumbach, N.; Neysadt, S.; Urban, A. S.; Feldmann, J. Fast Electron and Slow Hole Relaxation in InP-Based Colloidal Quantum Dots. *ACS Nano* **2019**, *13*, 14408–14415.
- (46) Nguyen, A. T.; Jen-La Plante, I.; Ippen, C.; Ma, R.; Kelley, D. F. Extremely Slow Trap-Mediated Hole Relaxation in Room-Temperature InP/ZnSe/ZnS Quantum Dots. *J. Phys. Chem. C* **2021**, *125*, 4110–4118.
- (47) Kim, T.; Won, Y.; Jang, E.; Kim, D. Negative Trion Auger Recombination in Highly Luminescent InP/ZnSe/ZnS Quantum Dots. *Nano Lett.* **2021**, *21*, 2111–2116.
- (48) Pandey, A.; Guyot-Sionnest, P. Slow Electron Cooling in Colloidal Quantum Dots. *Science* **2008**, *322*, 929–932.

- (49) Cragg, G. E.; Efros, A. L. Suppression of Auger Processes in Confined Structures. *Nano Lett.* **2010**, *10*, 313–317.
- (50) Bae, W. K.; Padilha, L. A.; Park, Y.-S.; McDaniel, H.; Robel, I.; Pietryga, J. M.; Klimov, V. I. Controlled Alloying of the Core–Shell Interface in CdSe/CdS Quantum Dots for Suppression of Auger Recombination. *ACS Nano* **2013**, *7*, 3411–3419.
- (51) Rabouw, F. T.; Vaxenburg, R.; Bakulin, A. A.; van Dijk-Moes, R. J. A.; Bakker, H. J.; Rodina, A.; Lifshitz, E.; Efros, A. L.; Koenderink, A. F.; Vanmaekelbergh, D. Dynamics of Intraband and Interband Auger Processes in Colloidal Core–Shell Quantum Dots. *ACS Nano* **2015**, *9*, 10366–10376.

□ Recommended by ACS

Observation of Phonon Cascades in Cu-Doped Colloidal Quantum Wells

Junhong Yu, Hilmi Volkan Demir, *et al.*
NOVEMBER 03, 2022
NANO LETTERS

READ

Area-Independence of the Biexciton Oscillator Strength in CdSe Colloidal Nanoplatelets

Carmelita Roda, Zeger Hens, *et al.*
NOVEMBER 21, 2022
NANO LETTERS

READ

Exciton Recycling in Triplet Energy Transfer from a Defect-Rich Quantum Dot to an Organic Molecule

Jie Zhang, Masanori Sakamoto, *et al.*
JULY 10, 2022
THE JOURNAL OF PHYSICAL CHEMISTRY C

READ

Parabolic Potential Surfaces Localize Charge Carriers in Nonblinking Long-Lifetime “Giant” Colloidal Quantum Dots

Marcell Pálmai, Preston T. Snee, *et al.*
DECEMBER 01, 2022
NANO LETTERS

READ

[Get More Suggestions >](#)